PAPER

Check for updates

Atomic-level investigation on the oxidation efficiency and corrosion resistance of lithium enhanced by the addition of two dimensional materials†

Md. Habibur Rahman, [ID] ‡*[a] Emdadul Haque Chowdhury [ID] ‡[a]
and Sungwook Hong [ID] *[b]

Understanding the oxidation and corrosion characteristics of Lithium (Li)-based systems is critical to their successful use as a solid fuel in spacecraft, powerplants, rechargeable batteries, submarines, and many other aquatic and corrosive environments. This study offers a systematic roadmap for engineering the oxidation efficiency and corrosion resistance of Li-based systems using ReaxFF-based Reactive Molecular Dynamics (RMD) simulations for the first time. First, we explored the oxidation mechanism of bare Li (Li/O_2) at 1200 K, noticing that the oxidation process quickly ceases due to the creation of a passive oxide film on the Li surface. Afterward, we examined the effect of introducing graphene-oxide (GO) to the oxidation process of Li/O_2. Interestingly, the inclusion of GO establishes a new reaction pathway between Li and O_2, thus significantly improving oxidation efficiency. Additionally, we realized that when the concentration of GO increases in the system, the oxidation rate of Li/O_2 increases considerably. As exposed to O_2 and H_2O, bare Li is observed to be highly corrosion-prone, while graphene (Gr)-coated Li exhibits excellent corrosion resistance, suggesting that Gr might be used as a promising corrosion-protective shield. Overall, this study is intended to serve as a reference for experimental investigations and assist researchers and engineers in designing more efficient Li-based functional systems.

1. Introduction

With the rising need for environmentally friendly and sustainable energy, prompted by the imperative to minimize greenhouse gas (CO_2, CH_4, NO) emissions in order to combat anthropogenic global warming, renewable energy sources such as wind and solar power systems have gained popularity.[1] However, large-scale power generation strategies are essential since the temporal accessibility of these green energy sources often falls short of meeting actual energy demand.[1] In that context, Lithium (Li) is an ideal candidate for storing energy in a combustion process.[1] Li, which has an atomic number (Z) of 3, and an atomic weight of 7 a.m.u., has an exceptionally low electronegativity and is located near hydrogen (H) on the periodic table.[2] Moreover, it contains a vast amount of chemical energy owing to the available valence shell electron relative to

[a]Department of Mechanical Engineering, Bangladesh University of Engineering and Technology, Dhaka, 1000, Bangladesh. E-mail: imd.habiburrahman@gmail.com

[b]Department of Physics and Engineering, California State University, Bakersfield, 93311, USA. E-mail: shong10@csub.edu

‡ These authors contributed equally to this work.

its mass, resulting in high specific energy.[1,2] In fact, after boron (B) and beryllium (Be), Li has the third-highest energy to mass ratio, referred to as specific energy (kJ kg^{-1}), among all alkali metals/metalloids.[1,3] Such high specific energy encourages its use as an anode material in Li/O_2, Li-ion, and Li/air batteries.[1] Additionally, Li is a well-established energy carrier and an element of processes that generate hydrogen *via* the Li–water interaction, Li hydrides, and borohydrides.[4–6] Also, Li has been proposed as fuel for submarines and rockets,[1] and it has been incorporated into underwater propulsion systems as a chemical fuel.[1,7,8]

Generally, metals have traditionally been known to be good energy storage resources in addition to being effective additives in slurry fuels, energetic materials, and propellants by virtue of their high specific energy.[3,9–23] The majority of prior research on harnessing the chemical energy contained in metal fuels has concentrated on the reaction of various metals, particularly aluminum (Al) and magnesium (Mg), with water to produce hydrogen on demand, with only a few studies focusing on the combustion of metal fuels to generate heat.[12–14] Lately, the combustion of Li with various gaseous products has piqued interest for a multitude of reasons. For instance, Li has been employed in nuclear fusion reactors as a tritium breeder

blanket and coolant.[1] Besides, Li fires have been studied extensively in order to gain a thorough understanding of the combustion mechanism.[1] When power is required, Li is combined with the exhaust from an air or power plant station to generate heat for thermal power plants.[1] Once there is adequate renewable energy, the combustion products of the solid phase can be recovered and recycled into elemental Li through electrolysis.[1] Furthermore, Li has been widely used in rechargeable batteries for electric cars and a wide variety of electronic gadgets such as mobile phones, notebook computers, and digital cameras.[24,25] Since Li-ion batteries have a large number of active electrodes with highly combustible electrolytes, heat is generated within the cell under abnormal conditions like overcharging or internal short circuits, which may lead to hazardous thermal runaway reactions in the worst-case scenario.[26] Most battery-driven accidents triggered by spontaneous combustion have occurred in recent years, including the fire of the 787 Boeing Dreamline batteries and the explosion of a Tesla Model S electric car in 2013.[25] As a result, the safety issue remains an impediment to the widespread use of Li batteries.[25]

On the other side, Gr and other two-dimensional (2D) sp^2 hybridized carbon materials are predicted to have a significant impact in the field of catalysis, thanks to their peculiar mechanical, electrical, thermal, and optical properties, as well as their high specific surface area relative to other carbon-based materials.[27–32] Geim et al. (2004), for the first time, successfully exfoliated single layer Gr from graphite.[28,29] Gr's extraordinary electronic properties, including the half-integer quantum Hall effect, superior charge carrier mobility due to its massless Dirac fermion nature, and especially quantum capacitance, render it one of the most useful materials in optoelectronic systems.[31–34] However, the high expense of synthesizing and characterizing Gr-based nanomaterials, such as the chemical vapor deposition process, oxidation/reduction protocols, etc., has impeded their use as catalytic support.[27–29] Nonetheless, "graphene oxide (GO)," a Gr analog with oxygenated functionalities on the surface, which is fabricated by graphite oxidation in the presence of strong oxidizing agents, has generated considerable attention in the nanocatalyst scientific community.[35] Additional chemical modifications to the GO surface could incorporate newer catalytically active sites that are critical for novel catalytic activities.[27,28]

In that context, GO and its chemically modified variants have been shown to be highly catalytic in various reactions, including oxidation and thermal decomposition.[27,28] For instance, Bielawski et al.[36] were the first to show GO's superior catalytic activity in liquid phase organic transformations. Since that time, a number of organic transitions have been investigated by incorporating functional groups onto the graphitic substrate.[28,36] Notably, carbon materials serve as specialized catalyst supports in heterogeneous catalysis by anchoring various active materials through their active sites and may even function as a catalyst on their own. Additionally, the physicochemical properties of carbon-based materials, such as tunable permeability and surface chemistry, make them suitable candidates for use as catalysts in a range of applications.[27,28]

Protecting the reactive metals' surfaces has become a priority for the scientific community. Nonetheless, traditional methods such as chemical modification,[37] anodization,[38] formation of oxide layers,[39] polymers,[40] paints and varnishes,[41] and coating with organic layers[42] have demonstrated a number of drawbacks, including the formation of waste products, limited chemical stability, susceptibility to damage by heat, and modification of the base metals' physical properties.[43] On the other hand, Gr has been repeatedly identified as an ideal material for corrosion inhibition owing to its exceptional thermal and chemical stability, as well as mechanical strength with minimal alteration of the base metals' physical properties.[43–46] Gr is the thinnest known corrosion-protecting coating and has a negligible effect on the total dimension of the coated metal.[43] It has exceptional optical transparency (about 2.3% absorption per layer[47]) in the visible spectrum, as well as outstanding electrical and thermal conductivity. Therefore, it has a minor alteration to the optical, thermal, and electric properties of the coated metal.[44] On top of that, under severe conditions, Gr remains stable and chemically inert to oxidizing gas and liquid solutions, while other substrates would suffer fast chemical reactions.[43,44] Along with its large specific surface area and six-membered ring structure, the Gr surface forms an ionically impermeable diffusion barrier that can effectively prevent charge transfer, significantly improving water permeability and corrosion attack.[43,44,46] Consequently, Gr has been studied experimentally as an anti-corrosive coating on a number of materials, including Ni, Cu, and steel.[44,45,48,49] Using electrochemical Tafel analysis and impedance spectroscopy, Prasai et al.[45] reported that CVD-deposited multilayer Gr is capable of reducing the corrosion rate of Ni by 20 times. Also, Gr-based materials for maritime corrosion resistance are studied from two perspectives: pure Gr substrates and Gr composite coatings.[45,46,50] While the usage of Gr to deter corrosion has been well studied experimentally in the past, research involving mechanistic understanding is few and far between.[50]

Li's high specific energy, coupled with its extremely low electronegativity and atomic weight, makes it promising for a wide range of applications, including spacecraft, powerplants, combustion, rechargeable batteries, nuclear reactors, and aquatic conditions such as submarines, undersea propulsion systems, and many other corrosive environments. As a consequence, engineering Li's oxidation efficiency and exploring strategies to safeguard it against corrosive species are crucial for ensuring its long-term vitality, which is the aim of this study. Molecular Dynamics (MD) simulations have been shown to be an effective tool for studying the behavior and reaction mechanisms of nanosystems at the atomic level.[51–56] In this light, we used ReaxFF-based RMD simulations to explore the oxidation essence of bare Li/O_2 and how the oxidation efficiency of Li can be engineered by utilizing GO ($Li/O_2/GO$). Furthermore, the corrosion resistance of Gr-coated Li (Gr/Li) against O_2 ($Li/Gr/O_2$) and H_2O ($Li/Gr/H_2O$) have been analyzed as well, which are crucial for the successful utilization of Li as solid fuel and rechargeable Li-based battery.

2. Computational method

The ReaxFF reactive force field for Li/C/H/O interactions[57] was used to evaluate the complete reaction process of Li/O$_2$, Li/O$_2$/GO, Li/Gr/O$_2$, Li/H$_2$O, and Li/Gr/H$_2$O. Notably, the potential developed by Bedrov *et al.*[57] can reasonably define all the systems; in other words, this force field can excellently capture the atomic interaction among Li/C/H/O. Readers are directed to ref. 57 for a better understanding of the force field employed in this work. It is noteworthy that the ReaxFF has been optimized for a wide variety of physical and chemical systems, and it has been verified that it can accurately predict such physical and chemical systems.[58,59] Additional information on the definition and more perception of the ReaxFF force field can be found in ref. 60. Note that the C–C bond length of Gr was computed as ~1.45 Å; C–C, C–H, and O–H bond length of GO had been estimated as ~1.43 Å, ~1.05 Å, and ~0.95 Å, respectively, which show excellent endorsement with prior first-principles calculations.[61] Besides, the lattice constant of Li was also anticipated to be ~3.55 Å, which is also in good agreement with previous reports.[62] Hence, we can say that the force field can reasonably capture the chemical events during the RMD simulations.

Analyses of all the reaction processes of RMD simulations with the aforementioned ReaxFF reactive force field were conducted with an open-source LAMMPS[63] package using a canonical NVT ensemble (constant number of atoms, constant volume, and constant temperature). We used a Noose Hoover thermostat with a damping coefficient of 25 fs.[58,59] We preferred the time step of 0.25 fs because the previous ReaxFF results demonstrated that such a time step could accurately capture the event during a chemical reaction.[58,59,64] While conducting all the ReaxFF simulations, periodic boundary conditions were applied in the *X* and *Y* directions, while a fixed wall boundary condition was chosen along the *Z* direction.[65] Note that the size of the bare Li system was chosen as 6.4 nm × 6.4 nm x 3.5 nm, and 400 O$_2$

molecules and 400 H$_2$O molecules were added during the simulations (Fig. 1). During the reaction process of Li/O$_2$/GO, 10 and 16 GO sheets were added, corresponding to 6.25 wt% and 10 wt%, respectively. Also, note that the size of the Gr sheet (single layer and bilayer) was chosen as 6.4 nm × 6.4 nm. It is worth mentioning that the interlayer distance between each layer of Gr has been considered as 0.35 nm. OVITO[66] was used to take all snapshots during the chemical reaction process in this report.

3. Results and discussions

3.1 Oxidation performance of Li and Li/GO

First of all, we analyzed the bond population of Li–O and Li–H as a function of time to illuminate the comprehensive reaction process of Li/O$_2$ and Li/O$_2$/GO (6.25 wt%), as well as the influence of GO on the oxidation rate of Li. Note that all the simulations were performed at 1200 K. RMD snapshots in Fig. 2(a) and (b), respectively, manifest the oxidation process of Li without and with the presence of GO. Fig. 2(c) depicts the bond population of Li–O for Li/O$_2$ and Li/O$_2$/GO systems. As can be seen from this graph, Li readily reacts with O$_2$, which is characterized by the formation of a large number of ionic bonds between Li and O atoms within a few fractions of a picosecond for both Li/O$_2$ and Li/O$_2$/GO. To gain further insight, the relative potential energy of bare Li was evaluated as a function of time for Li/O$_2$ and Li/O$_2$/GO.

Generally, metal oxidation occurs when an ionic chemical reaction takes place on the surface of the metal in the presence of O$_2$.[59] The metal, therefore, binds to the O^{2-} and forms an oxide layer.[59] Due to metals' low ionization energies, loosely bound valence electrons, and low electronegativity, they readily lose electrons to nonmetal atoms, rendering them highly reactive.[2,67] It is noteworthy that Li tends to be the least reactive metal in element group IA due to the proximity of the Li valence electron to the atomic nucleus.[2,68] As compared to other
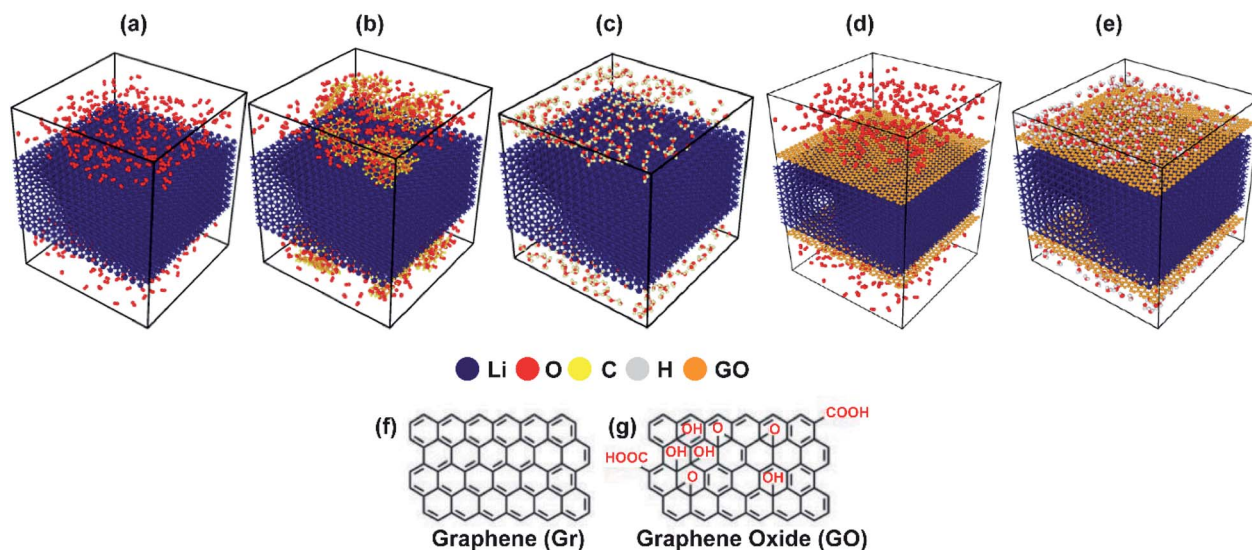

Fig. 1 Initial system of (a) Li/O$_2$ (b) Li/O$_2$/GO (c) Li/H$_2$O (d) Li/Gr/O$_2$, and (e) Li/Gr/H$_2$O, and schematics of (f) Gr and (g) GO.

elements in Group IA of the periodic table, Li burns less intensely in water than Na (sodium) and K (potassium), rendering it a promising solid fuel.[1,2] Nonetheless, Li is readily capable of forming ionic bonds with oxygen, which is also apparent in our RMD simulations (Fig. 2). Basically, the ionic bonds are formed between two atoms with a significant electronegativity difference.[2,67] Since anions are relatively more resilient than atoms, it would be much easier if the two types of elements could cooperate and address their energy problem.[2,67] To get more intuition on the reaction process, we can consider the following reaction.[1]

$$2 \text{ Li (aq)} + \tfrac{1}{2} O_2 \text{ (g)} \rightarrow Li_2O; \Delta H = -598 \text{ KJ mol}^{-1} \quad (1)$$

The O atom receives two electrons from two Li atoms and forms Li_2O. Notably, this exothermic reaction releases a large amount of thermal energy since the total energy of the products is less than the total energy of the reactants. It is worth remarking that exothermic reactions are ones that emit energy, usually in the form of heat or light.[1,2] Fig. 2(d) evinces that oxidation significantly reduces the potential energy of Li, which is indeed converted to thermal energy. The specific energy of this chemical reaction is ~43 MJ kg^{-1}; that is, burning of only 1 kg of Li will release ~43 MJ energy. We note that Li is much more reactive than Mg and Al.[1,2] For instance, the specific energy of $Mg + \tfrac{1}{2} O_2 \rightarrow MgO; \Delta H = -600$ KJ mol^{-1} and $2Al + 3/2 O_2 \rightarrow Al_2O_3; \Delta H = -1676$ KJ mol^{-1} is ~25 MJ kg^{-1} and ~32.3 MJ kg^{-1}, respectively. Mathematically, a huge amount of energy can be obtained by burning just 1 kg of Li relative to Mg and Al,

making it a promising solid fuel in spacecraft and areas where mass reduction of vehicles is a major concern. As seen in this figure, oxidation occurs spontaneously up to a small fraction of time, ~12 ps. Thereafter, the oxidation process seems to be stopped, as the bond population data does not differ over time. This can be attributed to the formation of an oxide coating (a passive film that serves as a shield to further chemical reactions on the surface of Li), which prevents the incoming O_2 molecules from coming into touch with the Li atoms, further clarified by the RMD snapshot in Fig. 2(a and b).

Following, we studied the effect of GO on the oxidation nature of Li/O_2. As shown in Fig. 2, the addition of GO vividly improves the oxidation rate of Li. As shown in Fig. 2(c), the addition of GO dramatically increases the amount of Li–O bonds produced during the oxidation of the Li/O_2/GO system, thus releasing more heat energy due to the creation of ionic bonds between Li–O. This is further corroborated in Fig. 2(d), which demonstrates that incorporating GO during the oxidation of Li seems to reduce the potential energy of the bare Li notably. Such a rapid decrease in potential energy caused by the addition of GO can also be attributed to the extra bond formation between Li–H, which also releases a significant amount of heat energy during the oxidation process, resulting in an overall improvement of energetic efficiency. Although oxidation of bare Li appears to be halted after a few fractions of time, i.e., the bond population of Li–O becomes constant due to the creation of the oxide coating on the Li surface, the addition of GO establishes a new reaction route between Li and O_2, allowing further O_2 molecules to come in contact with Li during the
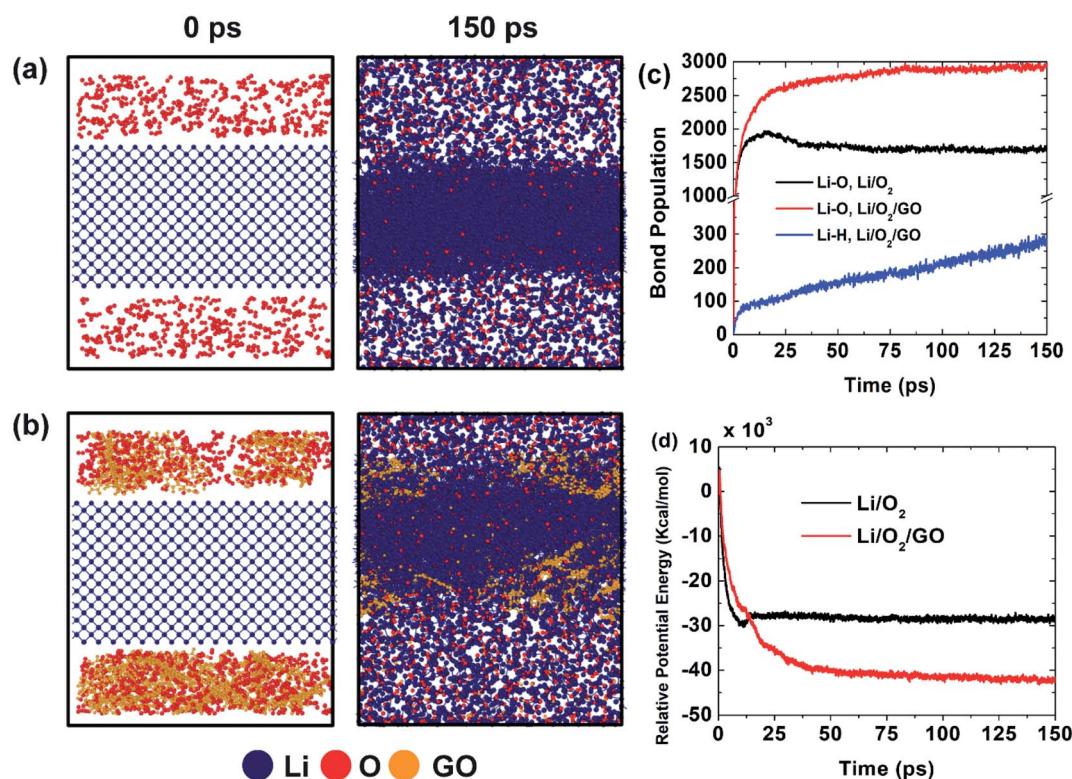

Fig. 2 RMD snapshots during the oxidation of (a) Li/O_2, (b) Li/O_2/GO. Variations of (c) bond population and (d) relative potential energy with time.
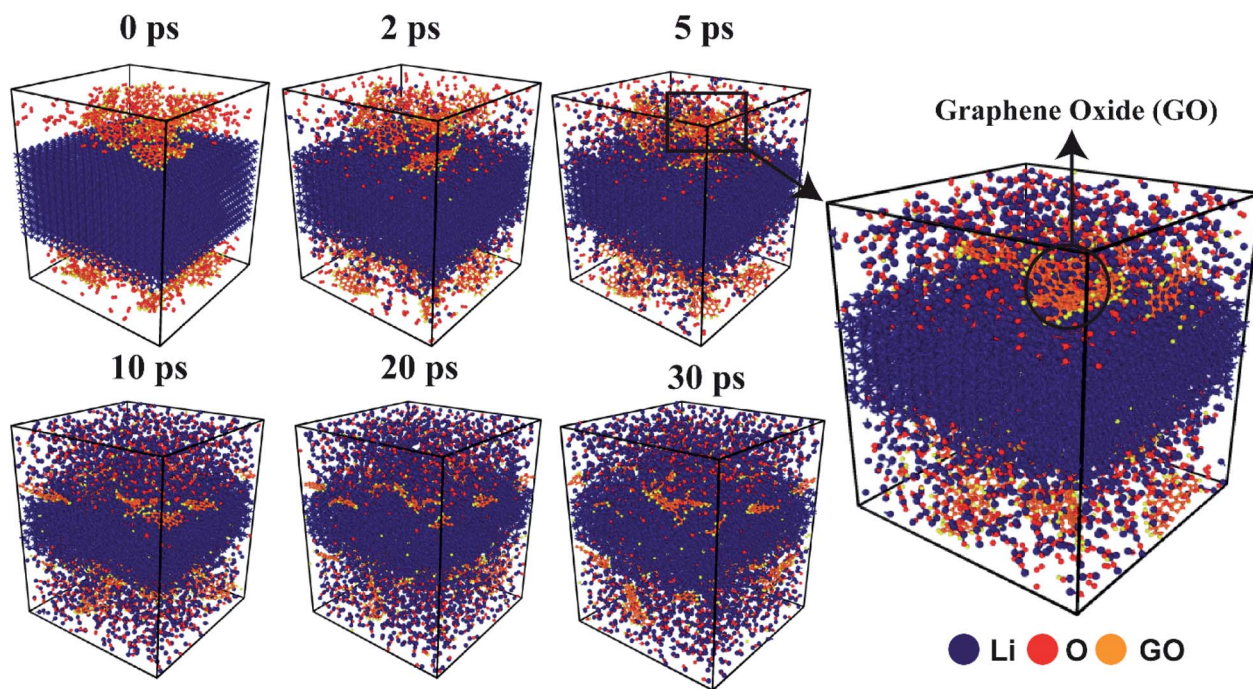
Fig. 3 RMD snapshots with zoomed inset during the oxidation of Li/O₂/GO at different time stages. Note that RMD results indicate that the addition of GO effectively prevents the formation of the passive layer on the Li surface during the oxidation process.

simulation process. This is endorsed by Fig. 2(c) and (d), which depict the exponential growth of Li–O bonds or exponential decay of potential energy of Li with time.

It is worth noting that O₂ molecules hardly penetrate the inner layer of the Li compared to the Li/O₂/GO system. Therefore, surface functional groups like epoxy (–C–O–C–), hydroxyl (–OH), and carboxyl (–COOH) make GO an excellent candidate for coordinating Li and O₂ molecules; additionally, GO serves as an effective anchoring site for immobilizing various catalytically active species.[27,28,69] Indeed, the surface of GO is decorated with at least five distinct O-containing functional groups, namely carboxyl (–COOH), hydroxyl (–OH), carbonyl (–C=O), epoxy (–C–O–C–), and ketone (–C=O).[27,69] These oxygenated groups endow four types of catalytic activity to GO such as (1) their acidic characteristics facilitate acid-catalyzed reaction; (2) their intermediary state interacts with oxidants, assisting in the acceleration of oxidation reactions; (3) their nucleophilic behavior facilitates binding reactions; and (4) their ideal π-conjugated form with significant deformities can stimulate a variety of catalytic activities.[27,69] Both the existence of O- containing functional groups on the GO surface and the π–π* network resulted in improved catalytic activity.[27] The existence of the π–π* network on the Gr surface facilitated the adsorption of substrate molecules onto the catalyst surface, and the O₂ functional groups stimulated the reaction.[27] In fact, in our RMD framework, GO serves as a bridge to connect Li and O₂ molecules. The reaction of Li/O₂/GO can be divided into the following steps: (i) initial interaction between Li, GO, and O₂ molecules; (ii) GO's penetrating into the sub-surface of bare Li; (iii) preventing the creation of passive layer on the surface of

bare Li; (iv) creating pores or cavities inside the Li that enables further O₂ molecules to come in contact with the inner region of Li. To gain more intuition on the oxidation of Li/O₂ and Li/O₂/GO, readers are referred to Movies 1 and 2 in the ESI.† In addition, zoomed inset of the chemical reaction of Li/O₂/GO at different time stages is provided in Fig. 3. Also, the effect of the concentration of GO has been added to the ESI† of this article.

3.2 Corrosion resistance of Li and Li/Gr against O₂ and H₂O

In this segment, we examined the corrosion resistance of bare Li and Gr-coated Li (Li/Gr) against O₂ and H₂O molecules. All the simulations were conducted at a temperature of 400 K. As mentioned earlier, Li is highly reactive and readily interacts with O₂ and H₂O even at low temperatures. As can be seen in the RMD snapshots of Fig. 4(a) and (b), Li is prone to corrosion when exposed to O₂ and H₂O, which is further evidenced by the bond population data for Li–O in Fig. 4(e) and (f). The advancement of next-generation batteries will necessitate the development of sustainable metallic Li anodes. However, the poor redox potential of Li renders it susceptible to corrosion, which must be fully understood before it can be used in practical energy storage systems.

Gr's chemical inertness is noteworthy (even to the extremely dangerous chemicals, such as HF), along with its impermeability to fluids and gases, rendering it an attractive corrosion-resistant shield material.[50] The key characteristics of a suitable corrosion-resistant surface barrier coating are (I) intrinsic protection to deterioration in a hostile environment, (II) efficient immunity to corrosive fluid penetration, and (III) structural stability over the coated component's expected lifespan.[50]
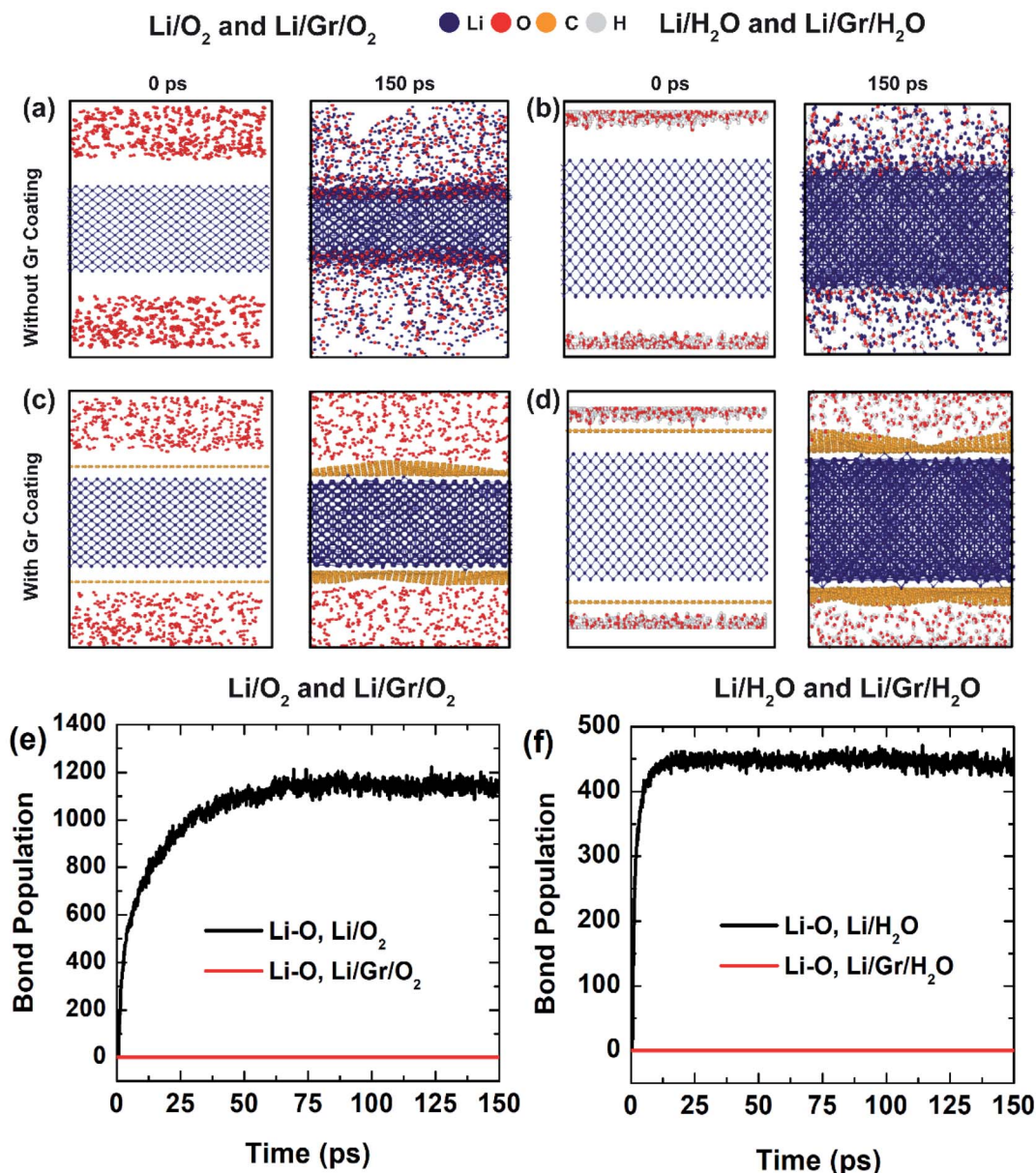
Fig. 4   RMD snapshots during the reaction of (a) Li/O$_2$, (b) Li/H$_2$O, (c) Li/Gr/O$_2$ (d) Li/Gr/H$_2$O. Variations of bond population data of Li−O for (e) Li/O$_2$ and Li/Gr/O$_2$, and (f) Li/H$_2$O and Li/Gr/H$_2$O systems with time.

It is well known that carbon-based materials (like graphite) are resistant to the majority of corrosive materials.[50] Nonetheless, due to their extreme brittleness, these materials are susceptible to mechanical failure and therefore have little application as coatings. A single layer of Gr, on the other hand, is confirmed to be extremely tough. By virtue of their toughness, mechanical stability, chemical inertness, and impermeability, the ultrathin Gr film is the thinnest known corrosion-protective coating.[50] Noticeably, oxidation of engineering alloys and energetic metals is a perplexing challenge to overcome, and conventional methods (such as appropriate alloying and coating) have only yielded modest improvements.[50] On the other side, a few layers of Gr coating on metals have been revealed to improve corrosion resistance significantly.[50,70] Given the high cost of corrosion,

novel approaches like long-term corrosion protection utilizing a Gr coating on such alloys are highly enticing.[46,50,70]

Following that, we coated the Li surface with Gr (Li/Gr) and performed entirely ReaxFF RMD simulations for 150 ps in the presence of ample O$_2$ and H$_2$O molecules to better grasp the corrosion behaviors of Li/Gr/O$_2$ and Li/Gr/H$_2$O. Interestingly, when the Li surface was entirely coated with Gr, no corrosion was observed, *i.e.*, no reaction between Li with O$_2$ and H$_2$O, as clarified by the RMD snapshots in Fig. 4(c) and (d). Additional evidence is provided in Fig. 4(e) and (f) by detailing the bond population data between Li−O when the Li surface is fully coated with Gr. Previously, Kirkland *et al.*[44] compared the corrosion resistance mechanisms of CVD Gr-coated Ni and Cu. Also, Prasai *et al.* reported a seven-fold increase,[45] while Raman

et al.[48] recorded a two-order-of-magnitude improvement. Interestingly, Prasai *et al.*[45,46] demonstrated that multilayer Gr sheets deposited on Ni using the CVD route minimize corrosion by a factor of twenty, which is far more than that claimed by Kirkland *et al.*[44] These prior studies are in excellent congruence with our ReaxFF RMD simulations concerning the superior corrosion resistance of Gr coatings.

The enhanced corrosion resistance could be ascribed to the exceptionally chemical inertness of Gr, thanks to its strongly coupled P_z molecular orbital remaining stable in a delocalized π bonding system, preventing Gr from forming covalent bonds with guest molecules.[46,50,70] Such an outstanding immunity to corrosion leveraging Gr coating can also be credited to its superior mechanical strength and durability even at extremely high temperatures.[46,50,70] Therefore, it can be inferred that Gr coatings can be applied to metal surfaces to effectively impede oxidation and corrosion owing to their chemical inertness as well as high-temperature endurance. Readers are directed to Movies 3 and 4 in the ESI† for a better understanding of the corrosion resistance of Li/Gr/O_2 and Li/Gr/H_2O. Also, the effect of thickness of Gr sheets has been added to the ESI† of this article.

4. Conclusions

In this assessment, we used ReaxFF-based RMD simulations to analyze the oxidation characteristics of bare Li/O_2 and the ways in which the oxidation efficiency and corrosion resistance of Li can be engineered by utilizing GO (Li/O_2/GO) catalysts and Gr coatings, respectively. Notably, our computed bond length data of Gr and GO, and the lattice parameter of Li showed excellent agreement with the literature. First, we exhaustively analyzed the oxidation process of Li/O_2 and Li/O_2/GO at 1200 K. The oxidation mechanism is observed to halt after a brief period of time owing to the formation of a passive oxide film on the Li surface, which prevents the incoming O_2 molecules from interacting with Li atoms. By comparison, the addition of GO creates a new reaction pathway between Li and O_2 and promotes further adsorption of O_2 molecules on the Li surface, significantly increasing the oxidation efficiency. Afterward, we examined the corrosion resistance of bare Li and Gr-coated Li (Li/Gr) against O_2 and H_2O molecules at 400 K. It is observed that Li reacts readily with O_2 and H_2O and is prone to corrosion even at low temperatures. Remarkably, when the Li surface was fully covered with Gr, no corrosion occurred even in the presence of high concentrations of O_2 and H_2O, indicating that Gr acted as an outstanding corrosion-protective shield owing to its chemical inertness, toughness, and impermeability. As such, this study provides a comprehensive guideline for engineering the oxidation efficiency and corrosion resistance of Li-based systems, which are crucial for the successful utilization of Li as a solid fuel in submarines, spacecraft, and next-generation energy storage systems.

Data Availability

The raw/processed data required to reproduce these findings may be available from the corresponding author upon reasonable request.

Conflict of interest

The authors declare that there is no conflict of interest.

Acknowledgements

References

1 M. Schiemann, J. Bergthorson, P. Fischer, V. Scherer, D. Taroata and G. Schmid, *Appl. Energy*, 2016, **162**, 948–965.

2 A. Bahl, *Essential of physical chemistry*, S Chand & Co Ltd, 2010.

3 J. M. Bergthorson, S. Goroshin, M. J. Soo, P. Julien, J. Palecka, D. L. Frost and D. J. Jarvis, *Appl. Energy*, 2015, **160**, 368–382.

4 J. Lu, Z. Z. Fang and H. Y. Sohn, *J. Power Sources*, 2007, **172**, 853–858.

5 Y. Wang, H. Li, P. He and H. Zhou, *ChemSusChem*, 2010, **3**, 571–574.

6 C. Li, P. Peng, D. W. Zhou and L. Wan, *Int. J. Hydrogen Energy*, 2011, **36**, 14512–14526.

7 E. G. Groff and G. M. Faeth, *J. Hydronaut*, 1978, **12**, 63–70.

8 S. H. Chan, *Prog. Energy Combust. Sci.*, 1993, **19**, 105–143.

9 T. Yabe, S. Uchida, K. Ikuta, K. Yoshida, C. Baasandash, M. S. Mohamed, Y. Sakurai, Y. Ogata, M. Tuji, Y. Mori, Y. Satoh, T. Ohkubo, M. Murahara, A. Ikesue, M. Nakatsuka, T. Saiki, S. Motokoshi and C. Yamanaka, *Appl. Phys. Lett.*, 2006, **89**, 261107.

10 H. Z. Wang, D. Y. C. Leung, M. K. H. Leung and M. Ni, *Renewable Sustainable Energy Rev.*, 2009, **13**, 845–853.

11 D. Wen, *Energy Environ. Sci.*, 2010, **3**, 591–600.

12 E. I. Shkolnikov, A. Z. Zhuk and M. S. Vlaskin, *Renewable Sustainable Energy Rev.*, 2011, **15**, 4611–4623.

13 M. S. Vlaskin, E. I. Shkolnikov, A. V. Bersh, A. Z. Zhuk, A. V. Lisicyn, A. I. Sorokovikov and Y. V. Pankina, *J. Power Sources*, 2011, **196**, 8828–8835.

14 Y. Yavor, S. Goroshin, J. M. Bergthorson, D. L. Frost, R. Stowe and S. Ringuette, *Int. J. Hydrogen Energy*, 2013, **38**, 14992–15002.

15 M. Schiemann, P. Fischer, V. Scherer, G. Schmid and D. Taroata, *Chem. Eng. Technol.*, 2014, **37**, 1600–1605.

16 A. Steinfeld, P. Kuhn, A. Reller, R. Palumbo, J. Murray and Y. Tamaura, *Int. J. Hydrogen Energy*, 1998, **23**, 767–774.

17 E. L. Dreizin, *Prog. Energy Combust. Sci.*, 2009, **35**, 141–167.

18 F. Maggi, S. Dossi, C. Paravan, L. T. DeLuca and M. Liljedahl, *Powder Technol.*, 2015, **270**, 46–52.

19 C. K. Law, *AIAA J.*, 2012, **50**, 19–36.

20 E. Shafirovich and A. Varma, *J. Propul. Power*, 2008, **24**, 385–394.

21 M. K. King, *J. Spacecr. Rockets*, 1985, **22**, 512–513.

22 W. Hao, L. Niu, R. Gou and C. Zhang, *J. Phys. Chem. C*, 2019, **123**, 14067–14080.

23 T. L. Connell Jr, R. A. Yetter, G. A. Risha, Z. J. Huba, A. Epshteyn and B. T. Fisher, *J. Propul. Power*, 2019, **35**, 662–665.

24 T. Tsujikawa, K. Yabuta, M. Arakawa and K. Hayashi, *J. Power Sources*, 2013, **244**, 11–16.

25 P. Huang, Q. Wang, K. Li, P. Ping and J. Sun, *Sci. Rep.*, 2015, **5**, 1–12.

26 Q. Wang, P. Ping, X. Zhao, G. Chu, J. Sun and C. Chen, *J. Power Sources*, 2012, **208**, 210–224.

27 F. Li, X. Jiang, J. Zhao and S. Zhang, *Nano Energy*, 2015, **16**, 488–515.

28 J. Pyun, *Angew. Chem., Int. Ed.*, 2011, **50**, 46–48.

29 Y. H. Jian, F. Ding, B. I. Yakobson, P. Lu, L. Qi and J. Li, *Proc. Natl. Acad. Sci. U. S. A.*, 2009, **106**, 10103–10108.

30 E. H. Chowdhury, M. H. Rahman, P. Bose, R. Jayan and M. M. Islam, *Phys. Chem. Chem. Phys.*, 2020, **22**, 28238–28255.

31 M. H. Rahman, E. H. Chowdhury, D. A. Redwan, S. Mitra and S. Hong, *Phys. Chem. Chem. Phys.*, 2021, **23**, 5244–5253.

32 E. H. Chowdhury, M. H. Rahman, S. Fatema and M. M. Islam, *Comput. Mater. Sci.*, 2021, **188**, 110231.

33 M. H. Rahman, S. Mitra, M. Motalab and P. Bose, *RSC Adv.*, 2020, **10**, 31318–31332.

34 Md. H. Rahman, E. H. Chowdhury, M. R. Bin Shahadat and M. M. Islam, *Comput. Mater. Sci.*, 2021, **191**, 110338.

35 B. Majumdar, D. Sarma and T. K. Sarma, in *Carbon-based nanofiller and their rubber nanocomposites*, Elsevier, 2019, pp. 425–439.

36 D. R. Dreyer, H.-P. Jia and C. W. Bielawski, *Angew. Chem., Int. Ed.*, 2010, **49**, 6686.

37 G. Grundmeier, C. Reinartz, M. Rohwerder and M. Stratmann, *Electrochim. Acta*, 1998, **43**, 165–174.

38 P. J. Kinlen, V. Menon and Y. Ding, *J. Electrochem. Soc.*, 1999, **146**, 3690.

39 V. K. Mittal, S. Bera, T. Saravanan, S. Sumathi, R. Krishnan, S. Rangarajan, S. Velmurugan and S. V. Narasimhan, *Thin Solid Films*, 2009, **517**, 1672–1676.

40 M. I. Redondo and C. B. Breslin, *Corros. Sci.*, 2007, **49**, 1765–1776.

41 D. M. Merkula, P. D. Novikov, V. N. Ivanenkov, V. V. Sapozhnikov and Y. I. Lyakhin, *Oceanol., USSR*, 1974, **14**, 299–300.

42 M. Stratmann, R. Feser and A. Leng, *Electrochim. Acta*, 1994, **39**, 1207–1214.

43 S. Chen, L. Brown, M. Levendorf, W. Cai, S.-Y. Ju, J. Edgeworth, X. Li, C. W. Magnuson, A. Velamakanni and R. D. Piner, *ACS Nano*, 2011, **5**, 1321–1327.

44 N. T. Kirkland, T. Schiller, N. Medhekar and N. Birbilis, *Corros. Sci.*, 2012, **56**, 1–4.

45 D. Prasai, J. C. Tuberquia, R. R. Harl, G. K. Jennings and K. I. Bolotin, *ACS Nano*, 2012, **6**, 1102–1108.

46 K. S. Aneja, H. M. Böhm, A. S. Khanna and S. Böhm, *FlatChem*, 2017, **1**, 11–19.

47 R. R. Nair, P. Blake, A. N. Grigorenko, K. S. Novoselov, T. J. Booth, T. Stauber, N. M. Peres and A. K. Geim, *Science*, 2008, **320**, 1308.

48 R. S. Raman, P. C. Banerjee, D. E. Lobo, H. Gullapalli, M. Sumandasa, A. Kumar, L. Choudhary, R. Tkacz, P. M. Ajayan and M. Majumder, *Carbon*, 2012, **50**, 4040–4045.

49 S. Sreevatsa, A. Banerjee and G. Haim, *ECS Trans.*, 2009, **19**, 259.

50 R. K. Singh Raman and A. Tiwari, *Jom*, 2014, **66**, 637–642.

51 E. H. Chowdhury, Md. H. Rahman, R. Jayan and M. M. Islam, *Comput. Mater. Sci.*, 2021, **186**, 110001.

52 Md. H. Rahman, E. H. Chowdhury and M. M. Islam, *J. Nanopart. Res.*, 2020, **22**, 311.

53 Md. H. Rahman, E. H. Chowdhury, D. A. Redwan and S. Hong, *Comput. Mater. Sci.*, 2021, **190**, 110272.

54 M. H. Rahman, M. S. Islam, M. S. Islam, E. H. Chowdhury, P. Bose, R. Jayan and M. M. Islam, *Phys. Chem. Chem. Phys.*, 2021, **23**, 11028–11038.

55 M. H. Rahman, E. H. Chowdhury and S. Hong, *Results Mater.*, 2021, **10**, 100191.

56 E. H. Chowdhury, M. H. Rahman and S. Hong, *Comput. Mater. Sci.*, 2021, **197**, 110580.

57 D. Bedrov, G. D. Smith and A. C. T. Van Duin, *J. Phys. Chem. A*, 2012, **116**, 2978–2985.

58 S. Hong and A. C. T. Van Duin, *J. Phys. Chem. C*, 2016, **120**, 9464–9474.

59 S. Hong and A. C. T. Van Duin, *J. Phys. Chem. C*, 2015, **119**, 17876–17886.

60 T. P. Senftle, S. Hong, M. M. Islam, S. B. Kylasa, Y. Zheng, Y. K. Shin, C. Junkermeier, R. Engel-Herbert, M. J. Janik, H. M. Aktulga, T. Verstraelen, A. Grama and A. C. T. Van Duin, *npj Comput. Mater.*, 2016, **2**, 1–14.

61 J. J. Hernández Rosas, R. E. Ramírez Gutiérrez, A. Escobedo-Morales and E. Chigo Anota, *J. Mol. Model.*, 2011, **17**, 1133–1139.

62 E. J. Covington and D. J. Montgomery, *J. Chem. Phys.*, 1957, **27**, 1030–1032.

63 S. Plimpton, *J. Comput. Phys.*, 1995, **117**, 1–19.

64 M. H. Rahman, E. H. Chowdhury and S. Hong, *Surf. Interfaces*, 2021, **26**, 101371.

65 Y. Jiang, S. Deng, S. Hong, J. Zhao, S. Huang, C. C. Wu, J. L. Gottfried, K. I. Nomura, Y. Li, S. Tiwari, R. K. Kalia, P. Vashishta, A. Nakano and X. Zheng, *ACS Nano*, 2018, **12**, 11366–11375.

66 A. Stukowski, *Modell. Simul. Mater. Sci. Eng.*, 2009, **18**, 015012.

67 A. Hofmann, *Physical Chemistry Essentials*, Springer International Publishing, 2018.

68 K. K. Kim, A. Hsu, X. Jia, S. M. Kim, Y. Shi, M. Hofmann, D. Nezich, J. F. Rodriguez-nieva, M. Dresselhaus, T. Palacios and J. Kong, *Nano Lett.*, 2011, **12**, 161–166.

69 B. Majumdar, D. Sarma and T. K. Sarma, in *Graphene Oxide – Applications and Opportunities*, InTech, 2018.

70 G. Wen, P. Bai and Y. Tian, *J. Bio- Tribo-Corros.*, 2021, 7, DOI: 10.1007/s40735-020-00456-6.